Title

Optical Detection and Sizing of Single Nanoparticles Using Continuous Wetting Films

Permalink

https://escholarship.org/uc/item/166964p9

Journal

ACS Nano, 7(9)

ISSN

1936-0851

Authors

Hennequin, Yves
Allier, Cédric P
McLeod, Euan
et al.

Publication Date

2013-09-24

DOI

10.1021/nn403431y

Peer reviewed

Optical Detection and Sizing of Single Nano-Particles Using Continuous Wetting Films

Yves Hennequin[1], **Cédric P. Allier**[1], **Euan McLeod**[3,4], **Onur Mudanyali**[3,4], **Daniel Migliozzi**[2], **Aydogan Ozcan**[3,4,5,6], and **Jean-Marc Dinten**[1]

[1]CEA, LETI, MINATEC, 17 rue des martyrs, 38054 Grenoble cedex 9, France

[2]École Polytechnique (member of ParisTech), 91128 Palaiseau, France

[3]Electrical Engineering Department, University of California, Los Angeles, California 90095, USA

[4]Bioengineering Department, University of California, Los Angeles, California 90095, USA

[5]California NanoSystems Institute, University of California, Los Angeles, California 90095, USA

[6]Department of Surgery, David Geffen School of Medicine, University of California, Los Angeles, California 90095, USA

Abstract

The physical interaction between nano-scale objects and liquid interfaces can create unique optical properties, enhancing the signatures of the objects with sub-wavelength features. Here we show that the evaporation on a wetting substrate of a polymer solution containing sub-micrometer or nano-scale particles creates liquid micro-lenses that arise from the local deformations of the continuous wetting film. These micro-lenses have properties similar to axicon lenses that are known to create beams with a long depth of focus. This enhanced depth of focus allows detection of single nanoparticles using a low magnification microscope objective lens, achieving a relatively wide field-of-view, while also lifting the constraints on precise focusing onto the object plane. Hence, by creating these liquid axicon lenses through spatial deformations of a continuous thin wetting film, we transfer the challenge of imaging individual nano-particles to detecting the light focused by these lenses. As a proof of concept, we demonstrate the detection and sizing of single nano-particles (100 and 200 nm), CpGV granuloviruses as well as *Staphylococcus epidermidis* bacteria over a wide field of view of *e.g.*, 5.10×3.75 mm^2 using a ×5 objective lens with a numerical aperture of 0.15. In addition to conventional lens-based microscopy, this continuous wetting film based approach is also applicable to lensfree computational on-chip imaging, which can be used to detect single nano-particles over a large field-of-view of *e.g.*, >20-30 mm^2. These results could be especially useful for high-throughput field-analysis of nano-scale objects using compact and cost-effective microscope designs.

Keywords

Wetting films; optical microscopy; computational imaging; nanoparticle detection; virus detection; bacteria imaging

Imaging and microscopy have been experiencing a renaissance over the last decade, where a significant portion of these advances provides new nano-imaging capabilities. In particular new label-free microscopy techniques are providing exciting paths to detect single nano-

particles down to 10 nm and viruses smaller than 100 nm in diameter.[1–14] These new optical tools can serve various applications in nano-technology, including imaging of self-assembly processes at the nano-scale and the characterization of nano-particle synthesis in terms of concentration, size and aggregation. However, all these approaches are relatively low throughput since they provide a limited imaging field of view (FOV), which is typically smaller than 0.1-0.2 mm^2. To improve this limited FOV of lens-based imaging systems, here we present a thin wetting film based approach where a nanoparticle embedded in a *continuous* wetting film creates a microscopic axicon lens that is able to condense light along its optical axis over distances up to three orders of magnitude greater than the size of the particle itself. We characterize the optical properties of these axicon lenses and show that the shape and the condensing power of such liquid lenses can be fine-tuned to enable the detection of nano-particles down to ∼100 nm using a low magnification microscope objective, achieving a large FOV of several mm^2. Note that these microscopic axicon lenses should not be confused with self-assembled isolated nano-lenses that have been recently demonstrated for coherent detection of nano-particles on a chip[15]. Here the physical origin is a local spatial deformations of a 'continuous' wetting film rather than formation of 'isolated' liquid refractive structures around each particle as in the case of nano-lenses. Besides detection of nano-particles using incoherent illumination and lens-based microscopy, we also demonstrate the simultaneous detection of single CpGV granuloviruses and *Staphylococcus epidermidis* bacteria over a wide field of view of *e.g.*, 5.10×3.75 mm^2 using a ×5 objective lens that has a numerical aperture of 0.15. These micro-scale axicon lenses also enable the detection of single 100 nm nanoparticles using computational lensfree imaging,[15-25] achieving an imaging FOV of *e.g.*, >20-30 mm^2.

Results and Discussion

Liquid axicon lenses

When a small amount of buffer solution is deposited on a wetting surface it spreads to form a flat drop that quickly evaporates leaving non-volatile solutes on the substrate. With a polymer or concentrated surfactant solution, the evaporation of a microliter drop will leave a nearly flat film at the center of the drop bounded eventually with a thicker edge near the initial contact line.[26] Additionally, if particles are dispersed in the solution they will be left as inclusions in the film, creating local spatial deformations of the interface provided their size is larger than the local film thickness. While the bulk of the film is totally transparent, these local deformations act as liquid axicon lenses that strongly condense light, providing a powerful means for detecting small particles.

First, the effect of the polymer film is demonstrated with relatively large 5μm particles. For this we evaporate droplets of 1 μL on a glass coverslip from two suspensions of beads with and without the dissolved polymer. We use conventional bright-field microscopy to make image-stacks, focusing at successive depths in order to image the light-cone produced by the beads (see Fig. 1). The condensing power of the liquid lens formed by the bead under the polymer film is evident: most of the light is focused on the optical axis forming an almost non-diffracting beam, characteristic of an axicon lens (see Fig. 1b). The direct consequence of this is that a significant contrast between the center of the interference pattern (local intensity maximum) and the image background persists up to distances of *millimeters* behind the liquid axicon lens. In contrast, a single bead without a polymer film focuses incoming light to a point at relatively short distances (see Fig. 1c). Beyond the focal point, the light cone rapidly expands while the on-axis intensity drops quickly to background level.

We can model and better understand these observations by computing the shape of the film with a spherical inclusion according to references [27–29] (see. Fig. 2). Assuming complete wetting of a particle of diameter D by a film of thickness h_0, the local height $\zeta(r)$ above h_0 of

the liquid meniscus around the particle is a solution of the Young-Laplace equation (see Supplementary Information):

$$\zeta(r) = -L \tan \Psi_C \frac{K_0\left(\frac{r}{L}\right)}{K_1\left(\frac{r_C}{L}\right)} \quad \text{(Eq. 1)}$$

where L is the characteristic transverse length over which this liquid interface is distorted,[28] ψ_c is the meniscus slope angle, r is the radial coordinate, r_c is the contact ring radius and K_j is the j-th modified Bessel function of the second kind. For micron-thick films $L = \sqrt{\gamma/\rho g}$ is the capillary length of the liquid which sets the size of the lens where γ is the film-air surface tension, ρ is the film density and g is the gravitational acceleration. L is typically in the millimeter range for our experimental conditions. Near the particle, *i.e.*, for $r \ll L$, Eq. 1 can be approximated by:[29]

$$\zeta(r) = -2z_c \left[\ln\left(\frac{r}{2L}\right) + \gamma_e \right] \quad \text{(Eq. 2)}$$

where z_c is the height of the spherical cap not covered by the liquid film and γ_e is the Euler-Mascheroni constant. The shape of the lens described in Eq. 2 is that of an *axicon* with a concave curved slanting side as discussed in[30]. When illuminated with *coherent* light, an axicon lens forms an almost non-spreading beam, focusing the light into a line along the optical axis over an extended distance.[30–32] On the other hand, in our lens-based experiments with *incoherent* light, the central spot is primarily formed through light concentration and refraction instead of coherent interference. From simple geometrical considerations the maximal focal length z_a is determined by the convergence of the optical rays that start at the outer edges of the axicon lens (see Fig. 2b):

$$z_a \approx \frac{L}{\tan(\alpha)} \approx \frac{L}{\phi_2 - \phi_1} \approx \frac{L}{(n-1)\phi_1} \approx \frac{L}{(n-1)\left|\frac{\partial\zeta}{\partial r}\right|_{r=L}} \approx \frac{L^2}{2(n-1)z_c} \quad \text{(Eq. 3)}$$

For our liquid axicon lenses, z_a can be nearly up to three orders of magnitude greater than the height of the microlens. In comparison, a single particle without the polymer film can only focus light at a distance approximately equal to its size *i.e.*, on the order of microns[33] (see Fig. 1c).

We now consider the case of nanoparticle detection. Here thinner films are required to make a visible inclusion in the wetting film due to presence of nano-particles. We note that for thinner wetting films, the main contribution to the capillary length L is now given by the disjoining pressure $\Pi(h)$ in the film such that $L = \sqrt{\gamma/(\rho g - \Pi')}$ where $\Pi' = (d\Pi/dh)_{h_0}$ [27] (see Supplementary Information). We assume that the disjoining pressure is determined by the van der Waals forces between the two interfaces of the film, $\Pi(h) = \frac{A}{6\pi h^3}$, with A being the Hamaker constant.[34] We find that for a typical liquid polymer film on glass, L decreases sharply from millimeters to tens of microns for sub-micrometer film thicknesses. Therefore, despite the scaling down of its dimensions, local film deformations produced by nanoparticles should still focus light over relatively large distances, up to a few millimeters eventually. We managed to obtain thinner wetting films by lowering the polymer concentration, enabling the detection of single nano-particles, *i.e.*, 200 nm and 100 nm

diameter beads, while still using a low magnification objective lens (see Fig. 3, ×5 objective with NA = 0.15). In order to better characterize the liquid lenses, we also performed image-stacks of the light intensity above and below the lens with higher magnification objectives (see Fig. 4b, ×50 objective, NA = 0.8). These characterization experiments once again confirmed that the light forms a slowly diverging cone with its shadow extending below the object plane. Figure 4 shows the influence of the polymer concentration on the optical properties of the liquid lenses. Surprisingly for polymer concentrations greater than or equal to 0.2 %, the on-axis intensity has a very consistent profile (see Fig.4b): it decreases almost linearly with the distance from the object. We note that these profiles are again similar to that of axicon-like lenses.[31] Remarkably, measured values of z_a are in the range of 1.3-2 mm. For instance, for D = 200 nm particles (see Fig. 3a) and a polymer concentration of 0.2 % v/v, we estimate z_a = 1.4 mm from the spread of the central spot. To detect even smaller particles, such as 50 nm particles, the film thickness would need to be reduced further, however at low polymer concentrations required for such thin films, dewetting poses a significant challenge. As such, we cannot yet observe isolated 50 nm particles. At polymer concentrations of 0.1 % v/v and lower, the depth of focus of the axicon lens reduces dramatically, even for larger particles (see Fig. 4b). This suggests a transition to a different lens shape; in fact the on-axis intensity profile now resembles that of a micro-droplet (Fig 1c). This might be due to the partial dewetting of the film because nanometer-thin polymer films formed at low polymer concentrations become unstable. To preserve film stability at these low polymer concentrations, additional surface effects may need to be accounted for and the film stability can be better controlled by improving sample preparation steps, which will be a point of focus for future work. We should emphasize that the stability of the thin wetting film is important to enhance the signal-to-noise ratio (SNR) when detecting particularly small single nanoparticles. Although the absolute intensity may be greater at lower polymer concentrations (0.1-0.2%), the background noise is also larger, thus limiting

the SNR. The signal-to-noise ratio can be calculated as $\mathrm{SNR} = \frac{I_{\max} - \mu}{\sigma}$, where $I_{\max}$ is the local intensity maximum, μ and σ are the mean intensity and standard deviation of the intensity in a background noise region. Figure 5 shows the influence of the polymer concentration on the measured SNR with 200 nm beads (×5 objective lens). At higher polymer concentrations (*e.g.*, 0.8%) the film is too thick and the condensing ability of the microlens is low. A coarse optimum is found at a PEG concentration of 0.4%, where the measured SNR is 22±5 (calculated for N=25 individual 200 nm particles). The SNR can be almost doubled to 37 by subtracting image focused above and below the microlens, taking advantage of the asymmetric shadow cone observed in Fig. 4b. Comparing the detection results from bright-field snapshots with those from fluorescence images, we find high detection efficiencies reaching ∼90 %, with sample sizes on the order of 10 particles over a wide FOV of 9.1 mm^2.

Particle sizing results

Because the on-axis intensity depends on the film thickness relative to the particle diameter, the brightness of the central spot is consequently an indicator of the particle size. Measurements performed on mixed samples containing particle sizes of 0.2, 0.5 and 1µm show a linear relationship between intensity and particle size (see Fig. 6). This method forms a simple way of sizing and evaluating different populations of objects within the same sample. As an example (see Figs. 6f, g), we have probed a heterogeneous sample containing bacteria (*Staphylococcus epidermidis*) and viruses (CpGV granulovirus). Based on the size calibration curve (see Fig. 6d inner graph), we can measure the granulovirus diameter to be 330±50nm and the *Staphylococcus epidermidis* to be between 0.7 and 1.3 µm. Indeed the nominal size/diameter of *Staphylococcus epidermidis* is approximately 0.5 - 1.0 µm.[35] Although the actual sizes of the granulovirus samples were not verified by *e.g.*, SEM, the

measured dimension are consistent with the literature values, *i.e.* 200-450 nm in length[38]. These proof of concept experiments shows that it is possible to trap and detect different size of nanoparticles within the same polymer layer. However when particles of different dimensions are too close to one another (distance <10 µm), the beads' signatures overlap due to the poor spatial resolution of the low-NA objective lens, preventing the detection of the smallest bead. When the close particles are of equal dimensions, it is possible to resolve beads that are only 3.5µm apart (see white arrow in Fig. 6ab).

Note that all the experiments conducted in this work have been performed with spherical particles. In the case of for example non-spherical objects such as various bacteria, we believe that similar contrast and depth of field related improvement factors as reported in our manuscript should be observed since the cross-sections of various rod shaped bacteria will still be circular which will possess similar refractive properties, at least for several diffraction planes. The 3D morphological differences due to non-spherical geometries of various objects would surely create modifications in the overall refractive behavior of the continuous wetting films, and these optical differences would be the subject of future analysis and experiments.

Lensfree on-chip imaging

The collimation effect of the axicon liquid lenses can also be seen when focusing hundreds of microns away from the sample plane because the intensity decreases slowly with distance. Therefore at the optimal polymer concentration (0.4%) we were also able to detect nanoparticles in a lensfree on-chip imaging setup (see supplementary information).[16-18] In this setup, the imaging detector is a bare CMOS sensor (active area: 6.12×4.59 mm^2) without using imaging lenses. The distance between the coverslip and the sensor surface is on the order of 500 µm. Without magnification, this lensfree imaging setup is able to detect single 100 nm particles across a very large field of view of ~ 28 mm^2 (see Fig. S3). For each particle, the partially coherent diffraction pattern that is sampled at the detector plane has a FWHM of 20µm with an SNR of ~ 5.

Conclusions

In summary we have described a simple, yet effective way of detecting nanoscale objects (*e.g.*, $\sim$100-200 nm) over a large field-of-view. Creating spatial deformations on a continuous thin wetting film that behave as individual axicon lenses, nano-scale objects are detected using lens-based wide-field imaging configurations. The liquid axicon lenses have a high condensing ability along their optical axis, providing an opportunity for multiplexed detection of nano-scale particles and the estimation of their population levels within a liquid sample. This wetting-film-enabled detection of nano-objects across a wide field-of-view creates new opportunities, especially for opto-fluidic systems and may lead to new device concepts toward bringing nano-imaging capabilities to field settings and remote locations.

Methods

Sample preparation

Samples are prepared by mixing aqueous stock solutions, polymer (PEG 600, Sigma-Aldrich), surfactant (Tween 20 or Pluronic F68 with $c_s \sim 1$ CMC, Sigma-Aldrich) and particles (Fluorescent carboxyl-modified latex beads, Sigma-Aldrich). Deionized water is always filtered through disposable syringe filters with a pore size of 0.2 µm. The proportions of stock solutions are adjusted to reach the critical micelle concentration of the surfactant and a number of particles of $\sim 5 \times 10^3$ particles/µL. Microliter drops are simply placed on the cover glasses and left to evaporate at room temperature (20 °C). In order to form the wetting

film, a microliter drop is deposited on a glass coverslip that was previously cleaned and rendered hydrophilic such that the contact angle of the drop is typically below 5°. Formation of the film proceeds by evaporation of the water: the contact line is first pinned after which an apparent contact line recedes while leaving a film of surfactant and polymer with the particles as inclusions.

Substrate

For the glass substrate we use standard cover glasses (Corning) which are sonicated for approximately 10 min. in a soap solution, then rinsed with deionized water, acetone, isopropanol and dried with nitrogen. The cover glasses are subsequently placed for 30 seconds into oxygen plasma. This results in clean hydrophilic glass. Contact angles for water and polymer solutions are too low to be measured precisely but are below 5° (Kruss DSA100).

Microscopy and lensfree on-chip imaging

We observe the dried drops with bright-field and fluorescence microscopy (Olympus Provis AX70) with low magnification objectives ($\times 5$ $NA = 0.15$ and $\times 10$ $NA = 0.3$). To confirm that the revealed spots indeed correspond to the nanoparticles of interest, we used fluorescence microscopy to verify the locations of the particles against possible false positives from residual dust. In order to image the light cone, we make image-stacks at high magnification (Zeiss AxioPlan, $\times 50$ $NA = 0.8$). For lens-less imaging, we place the cover glass on a bare CMOS sensor (a 10MPixel $1/2.3''$ Aptina sensor) at a distance of 500 μm. The drop is illuminated with a red laser diode (650 nm, 3mW) placed approximately 20 cm above the sensor. Intensity profiles are extracted using image analysis software (ImageJ, MatLAB). The on-axis intensity profile for each polymer concentration is computed by averaging the profiles of at least ten microlenses.

Associated contents—Extended calculations of the shape of the liquid microlenses with corresponding figures. Contrast enhancement with a continuous wetting film and corresponding figures. Lensfree imaging of 100 nm particles with continuous thin wetting film and corresponding figures. Movie 1 shows in real-time the evaporation of a droplet with 200nm particles as seen in a mixed bright-field and fluorescence microscopy ($\times 10$ $NA = 0.3$). Movie 2 shows in real-time a close up on the moving evaporative front of a droplet with 200 nm particles as seen in bright-field microscopy. This material is available free of charge *via* the Internet at http://pubs.acs.org.

Supplementary Material

Refer to Web version on PubMed Central for supplementary material.

Acknowledgments

References

1. Lindfors K, Kalkbrenner T, Stoller P, Sandoghdar V. Detection and Spectroscopy of Gold Nanoparticles Using Supercontinuum White Light Confocal Microscopy. Phys Rev Lett. 2004; 93:037401-1–037401-4. [PubMed: 15323866]

2. Jacobsen V, Stoller P, Brunner C, Vogel V, Sandoghdar V. Interferometric Optical Detection and Tracking of Very Small Gold Nanoparticles at a Water-Glass Interface. Opt Express. 2006; 14:405–414. [PubMed: 19503354]

3. Daaboul GG, Yurt A, Zhang X, Hwang GM, Goldberg BB, Unlu MS. High-Throughput Detection and Sizing of Individual Low-Index Nanoparticles and Viruses for Pathogen Identification. Nano Lett. 2010; 10:4727–4731. [PubMed: 20964282]

4. Celebrano M, Kukura P, Renn A, Sandoghdar V. Single-Molecule Imaging by Optical Absorption. Nat Photonics. 2011; 5:95–98.

5. Wang G, Stender AS, Sun W, Fang N. Optical Imaging of Non-Fluorescent Nanoparticle Probes in Live Cells. Analyst. 2010; 135:215–221. [PubMed: 20098755]

6. Deutsch B, Beams R, Novotny L. Nanoparticle Detection Using Dual-Phase Interferometry. Applied Optics. 2010; 49:4921–4925. [PubMed: 20830181]

7. Kador L, Latychevskaia T, Renn A, Wild U. Absorption Spectroscopy on Single Molecules in Solids. J Chem Phys. 1999; 111:8755–8758.

8. Butter JYP, Hecht B, Crenshaw BR, Weder C. Absorption and Fluorescence of Single Molecules. J Chem Phys. 2006:154710-1–154710-5. [PubMed: 17059286]

9. Gerhardt I, Wrigge G, Bushev P, Zumofen G, Pfab R, Sandoghdar V. Strong Extinction of a Laser Beam by a Single Molecule. Phys Rev Lett. 2007:033601-1–033601-5. [PubMed: 17358681]

10. Tokeshi M, Uchida M, Hibara A, Sawada T, Kitamori T. Determination of Subyoctomole Amounts of Nonfluorescent Molecules Using a Thermal Lens Microscope: Subsingle Molecule Determination. Anal Chem. 2001; 73:2112–2116. [PubMed: 11354498]

11. Gaiduk A, Yorulmaz M, Ruijgrok PV, Orrit M. Room-Temperature Detection of a Single Molecule's Absorption by Photothermal Contrast. Science. 2010; 330:353–356. [PubMed: 20947760]

12. Wang Z, Guo W, Li L, Luk'yanchuk B, Khan A, Liu Z, Chen Z, Hong M. Optical Virtual Imaging at 50 nm Lateral Resolution with a White-Light Nanoscope. Nat Commun. 2011; 2:1–13. Article number 218.

13. Szameit A, Shechtman Y, Osherovich E, Bullkich E, Sidorenko P, Dana H, Steiner S, Kley EB, Gazit S, Cohen-Hyams T, et al. Sparsity-Based Single-Shot Subwavelength Coherent Diffractive Imaging. Nat Mater. 2012; 11:455–459. [PubMed: 22466747]

14. Wang Z, Millet L, Mir M, Ding H, Unarunotai S, Rogers J, Gillette MU, Popescu G. Spatial Light Interference Microscopy (SLIM). Opt Express. 2011; 19:1016–1026. [PubMed: 21263640]

15. Mudanyali O, McLeod E, Luo W, Greenbaum A, Coskun AF, Hennequin Y, Allier CP, Ozcan A. Wide-Field Optical Detection of Nano-Particles Using On-Chip Microscopy and self-Assembled Nano-Lenses. Nat Photonics. 2013; 7:247–254.

16. Repetto L, Piano E, Pontiggia C. Lensless Digital Holographic Microscope with Light-Emitting Diode Illumination. Opt Lett. 2004; 29:1132–1134. [PubMed: 15182009]

17. Mudanyali O, Tseng D, Oh C, Isikman SO, Sencan I, Bishara W, Oztoprak C, Seo S, Khademhosseini B, Ozcan A. Compact, Light-Weight and Cost-Effective Microscope Based on Lensless Incoherent Holography for Telemedicine Applications. Lab Chip. 2010; 10:1417–1428. [PubMed: 20401422]

18. Sikman SO, Sencan I, Mudanyali O, Bishara W, Oztoprak C, Ozcan A. Color and Monochrome Lensless On-Chip Imaging of *Caenorhabditis elegans* over a Wide Field-of-View. Lab Chip. 2010; 10:1109–1112. [PubMed: 20390127]

19. Allier CP, Hiernard G, Poher V, Dinten JM. Bacteria Detection with Thin Wetting Film Lensless Imaging. Biomed Opt Express. 2010; 1:762–770. [PubMed: 21258507]

20. Allier CP, Poher V, Coutard JG, Hiernard G, Dinten JM. Thin Wetting Film Lensless Imaging. Proc SPIE – Int Soc Opt Eng. 2011:7906–7914.

21. Psaltis D, Quake SR, Yang C. Developing Optofluidic Technology through the Fusion of Microfluidics and Optics. Nature. 2006; 442:381–386. [PubMed: 16871205]

22. Cui X, Lee LM, Heng X, Zhong W, Sternberg PW, Psaltis D, Yang C. Lensless High-Resolution On-chip Optofluidic Microscopes for *Caenorhabditis elegans* and Cell Imaging. Proc Natl Acad Sci U S A. 2008; 105:10670–10675. [PubMed: 18663227]

23. Schmidt H, Hawkins AR. The Photonic Integration of Non-Solid Media Using Optofluidics. Nat Photonics. 2011; 5:598–604.

24. Zheng G, Lee SA, Yang S, Yang C. Sub-Pixel Resolving Optofluidic Microscope for On-Chip Cell Imaging. Lab Chip. 2010; 10:3125–3129. [PubMed: 20877904]

25. Mudanyali O, Bishara W, Ozcan A. Lensfree Super-Resolution Holographic Microscopy Using Wetting Films on a Chip. Opt Express. 2011; 19:17378–17389. [PubMed: 21935102]

26. Deegan RD, Bakajin O, Dupont TF. Capillary Flow as the Cause of Ring Stains from Dried Liquid Drops. Nature. 1997; 389:827–829.

27. Kralchevsky PA, Nagayama K. Capillary Interactions between Particles Bound to Interfaces, Liquid Films and Biomembranes. Adv Colloid Interface Sci. 2000; 85:145–192. [PubMed: 10768480]

28. Fiegel J, Jin F, Hanes J, Stebe K. Wetting of a Particle in a Thin Film. J Colloid Interface Sci. 2005; 291:507–514. [PubMed: 15946673]

29. Di Leonardo R, Saglimbeni F, Ruocco G. Very-Long-Range Nature of Capillary Interactions in Liquid Films. Phys Rev Lett. 2008; 100:106103-1–106103-4. [PubMed: 18352212]

30. Lit JWY, Tremblay R. Focal Depth of a Transmitting Axicon. J Opt Soc Am. 1973; 63:445–449.

31. McLeod JH. The Axicon - a New Type of Optical Element. J Opt Soc Am. 1954; 44:592–597.

32. Durnin J, Miceli JJ, Eberly JH. Diffraction-Free Beams. Phys Rev Lett. 1987; 58:1499–1501. [PubMed: 10034453]

33. Born M, Wolf E. Principles of Optics: Electromagnetic Theory of Propagation, Interference and Diffraction of Light. Cambridge University Press. 1997

34. Israelachvili JN. Intermolecular and Surface Forces. Academic Press Inc. 1991

35. Schleifer KH, Kloos WE. Isolation and Characterization of *Staphylococci* from Human Skin I. Amended Descriptions of *Staphylococcus epidermidis* and *Staphylococcus saprophyticus* and Descriptions of Three New Species: *Staphylococcus cohnii*, *Staphylococcus haemolyticus*, and *Staphylococcus xylosus.* Int J Syst Evol Microbiol. 1975; 25:50–61.

36. De Gennes PG, Brochart-Wyart F, Quéré D. Capillary and Wetting Phenomena: Drops, Bubbles, Pearls, Waves. Springer Science & Business Media, Inc. 2004; Chapter 2

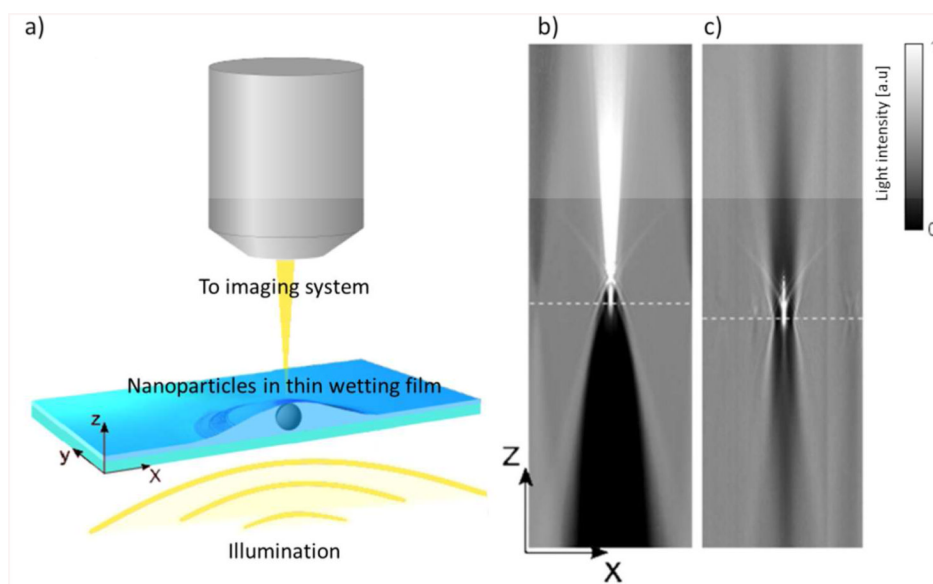37. Capinera, John. Encyclopedia of Entomology. Springer Edition. 2008

Figure 1.
(a) Schematic of a liquid axicon lens consisting of a continuous liquid film wetting a microparticle (not to scale). The liquid lenses are formed by the evaporation of the water from aqueous suspensions containing dissolved polymer. This can be realized by simple drop evaporation on glass coverslips. The liquid lenses focus light primarily along the optical axis. (b) Microscopic image of the light cone produced by the liquid lens formed with a 5μm diameter particle and reconstructed from microscopic image-stacks. The image dimension is 15 μm × 500 μm and the dash-line indicates the position of the particle. (c) Same as in (b), but without the wetting film.
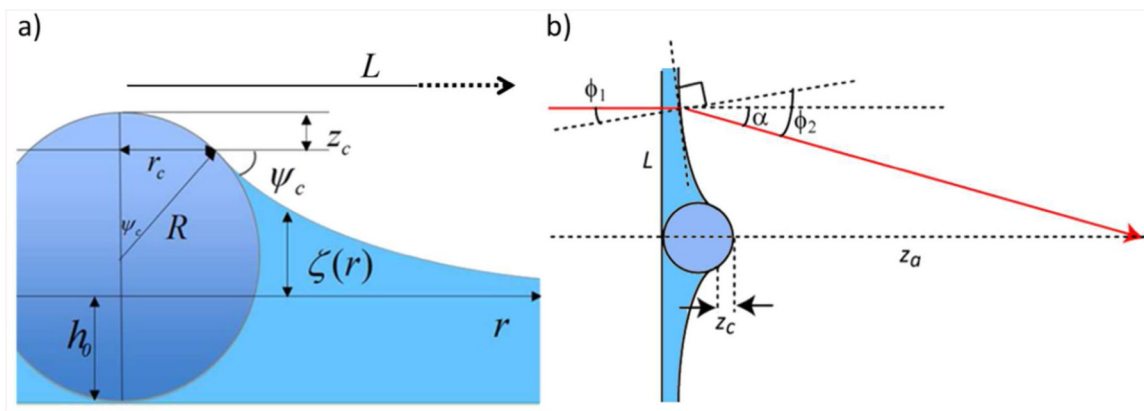
Figure 2.
(a) Schematic representation of a particle in the polymer film spread on a flat substrate. R is the radius, h_0 is the thickness of the film far away from the particle, z_c is the height of the spherical cap not covered by the liquid film, $\zeta(r)$ is the height of the liquid meniscus, such that $\lim_{r \to \infty} \zeta(r) = 0$. (b) Schematic of how the liquid axicon lens refracts a normal-incidence light ray (red).
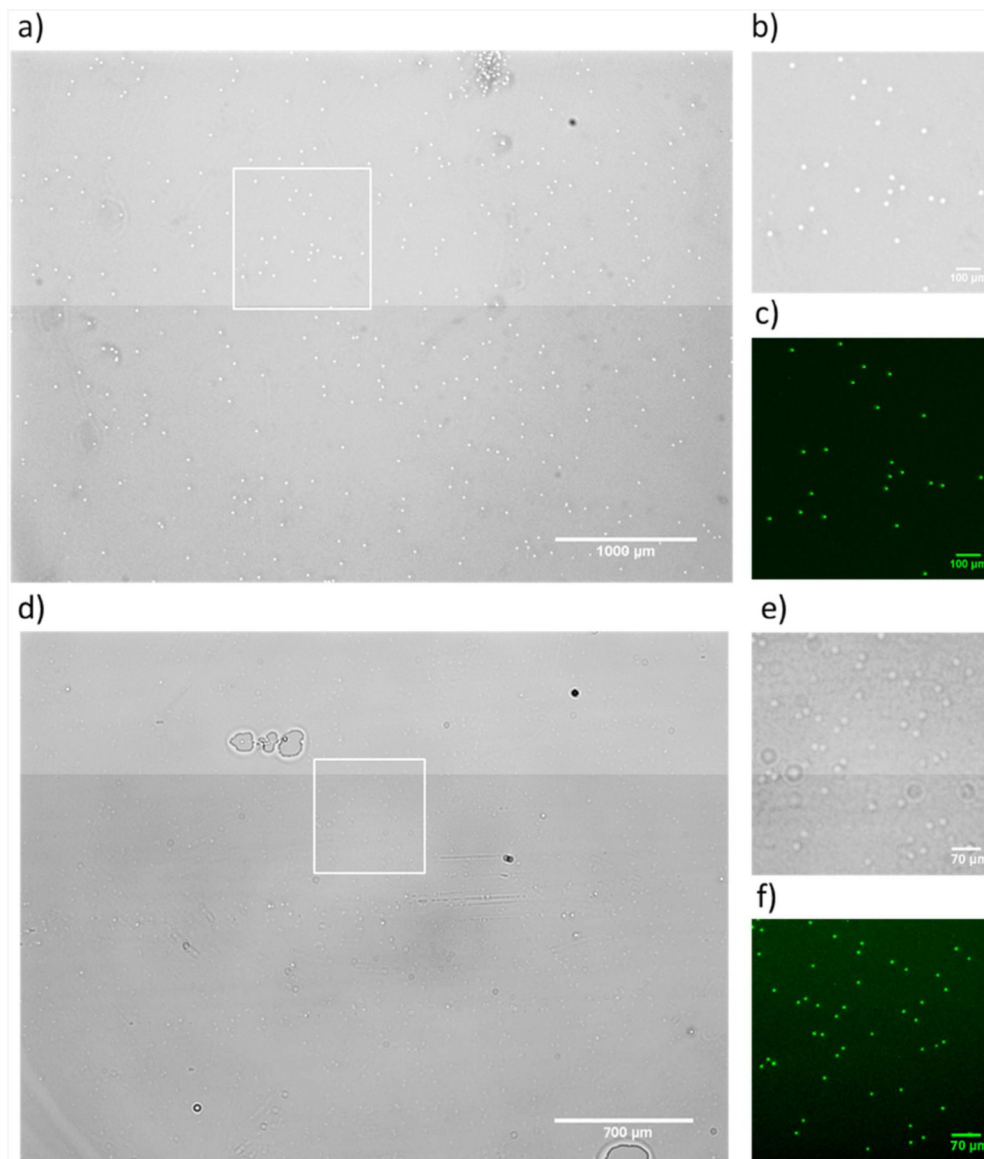
Figure 3.
(a) Bright field microscopic image of an evaporated drop with polymer (PEG 0.4% v/v) and 200 nm particles taken at ~100μm above the drop (×5 objective, NA = 0.15, ×1.76 effective magnification, FOV of 19.1mm^2). Because of the liquid lenses formed by the polymer on top of the particles, the latter can be seen as white spots in the center of the drop despite the low magnification and large field-of-view (5.10 mm × 3.75 mm). (b) Close-up of the area indicated in (a). (c) The same area is shown under fluorescence microscopy. (d) An evaporated drop with polymer (PEG 0.2% v/v) and 100 nm diameter particles (×5 objective, NA = 0.15, ×2.5 effective magnification, FOV of 9.4 mm^2). The white square has a side length of 0.66 mm, a close-up of which is shown in (e) in bright field conditions and in (f) in fluorescence.
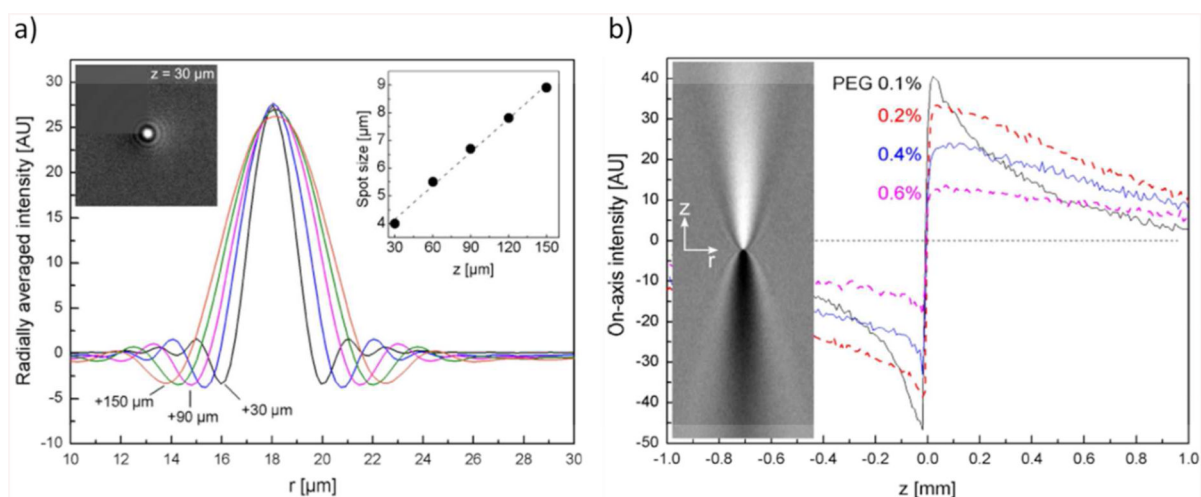
Figure 4.
Optical characterization of the axicon liquid lenses that are formed by 200 nm particles in continuous PEG films. (a) Transverse intensity modulations as various focus depths. The curves are obtained by radially averaging the intensity from the center of the particle, see top-left quadrant in the upper-left inset, which shows the interference pattern produced 30 µm above a 200 nm particle. The image width is 26 µm. The central spot spreads linearly with the distance from the particle (upper-right inset). (b) On-axis intensity profiles for liquid lenses obtained by evaporating suspensions of varying PEG concentrations. The image shows the light cone reconstructed from 2D images of the liquid lens in (a). Image dimensions are 26 µm × 2000 µm.

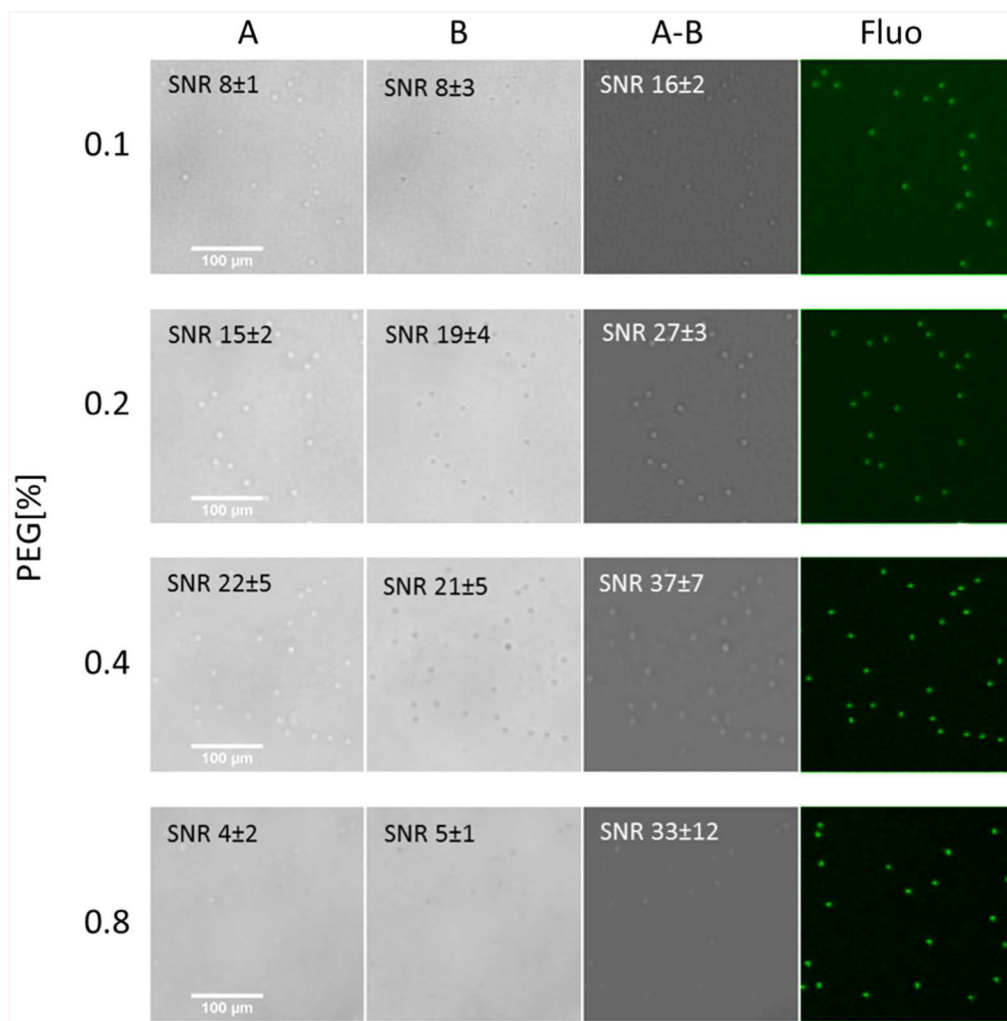**Figure 5.**
Microscope images (×5 objective lens) focused at ∼200 μm above (A) or below (B) the 200nm particle plane for various PEG polymer concentrations. The signal-to-noise ratio is calculated as $\mathrm{SNR} = \dfrac{\mathrm{I}_{\max} - \mu}{\sigma}$, where $\mathrm{I}_{\max}$ is the local intensity maximum, μ and σ are the mean intensity and standard deviation of the intensity in a background noise region. The SNR almost doubles by subtracting the images focused above and below the particle plane, *i.e.*, (A-B).
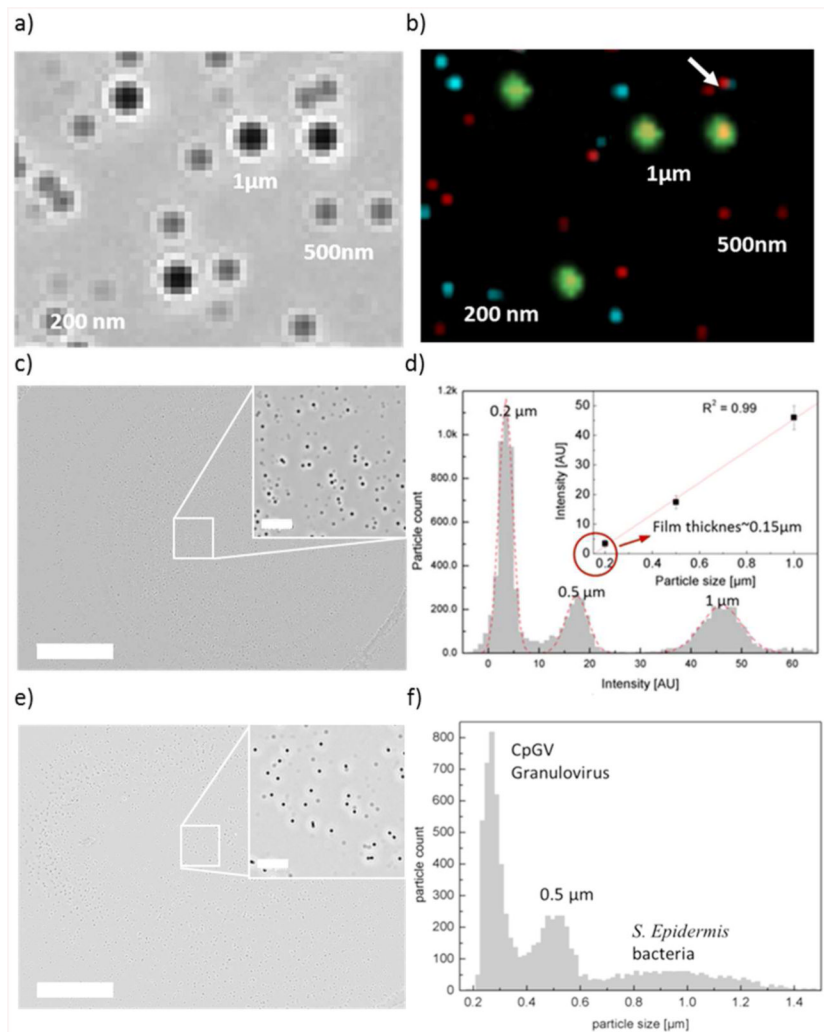
Figure 6.
(a) Details of a 19.1 mm^2 FOV bright field microscopic image (×5 objective, NA = 0.15) of an evaporated drop with continuous polymer thin film and 200nm, 500nm and 1μm beads. For comparison purposes, the fluorescence microscopy image (×5 objective, NA = 0.15) is shown in (b) with a color coding the different type of beads: 1μm in green, 500nm in red and 200nm in blue. (c) Bright field microscopic image (×5 objective, NA = 0.15) of an evaporated drop with continuous polymer thin film and 200nm, 500nm and 1μm beads. Scale bar is 1000μm (100 μm for the inset). (d) Local maxima intensity distribution measured on the image (c). The red curves show the Gaussian fits of the intensity peaks of the different particle patterns, respectively that of 200nm, 500 nm and 1μm beads. The inner graph shows the plot of the local maxima intensity as a function of the particle diameters, respectively 200nm, 500 nm and 1μm. The error bars represent the standard deviation of the local maxima intensity. (e) Bright field microscopic image (×5 objective, NA = 0.15) of an evaporated drop with continuous polymer thin film and CpGV, ~1μm *Staphylococcus epidermidis* bacteria and 500nm beads. Scale bar is 1000μm (100 μm for the inset). (f) Local maxima intensity distribution measured on the image (e). The inner plot in (d) serves as calibration curve to plot the maxima distribution as a function of the particle size.